

**RL-TR-96-64**  
**Final Technical Report**  
**July 1996**



# **A STUDY OF POLED FILMS OF ADVANCED ELECTROOPTIC POLYMERS**

**Washington University**

**Robert R. Krchnavek and Daniel Rode**

19961022 084

*APPROVED FOR PUBLIC RELEASE; DISTRIBUTION UNLIMITED.*

**DTIC QUALITY INSPECTED 4**

**Rome Laboratory**  
**Air Force Materiel Command**  
**Rome, New York**

This report has been reviewed by the Rome Laboratory Public Affairs Office (PA) and is releasable to the National Technical Information Service (NTIS). At NTIS it will be releasable to the general public, including foreign nations.

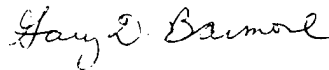
RL-TR-96-64 has been reviewed and is approved for publication.

APPROVED:



RAYMOND K. BONCEK  
Project Engineer

FOR THE COMMANDER:



GARY D. BARMORE  
Major, USAF  
Deputy Director of Surveillance & Photonics

If your address has changed or if you wish to be removed from the Rome Laboratory mailing list, or if the addressee is no longer employed by your organization, please notify RL/OCPA, 25 Electronic Pky, Rome, NY 13441-4514. This will assist us in maintaining a current mailing list.

Do not return copies of this report unless contractual obligations or notices on a specific document require that it be returned.

REPORT DOCUMENTATION PAGE			Form Approved OMB No. 0704-0188	
<small>Public reporting burden for this collection of information is estimated to average 1 hour per response, including the time for reviewing instructions, searching existing data sources, gathering and maintaining the data needed, and completing and reviewing the collection of information. Send comments regarding this burden estimate or any other aspect of this collection of information, including suggestions for reducing this burden, to Washington Headquarters Services, Directorate for Information Operations and Reports, 1215 Jefferson Davis Highway, Suite 1204, Arlington, VA 22202-4302, and to the Office of Management and Budget, Paperwork Reduction Project (0704-0188), Washington, DC 20503.</small>				
1. AGENCY USE ONLY (Leave blank)	2. REPORT DATE July 1996	3. REPORT TYPE AND DATES COVERED Final Feb 95 - Feb 96		
4. TITLE AND SUBTITLE  A STUDY OF POLED FILMS OF ADVANCED ELECTROOPTIC POLYMERS		5. FUNDING NUMBERS  C - F30602-95-C-0024 PE- 62702F PR- 4600 TA- P4 WU- PJ		
6. AUTHOR(S)  Robert R. Krchnavek Daniel L. Rode		8. PERFORMING ORGANIZATION REPORT NUMBER  N/A		
7. PERFORMING ORGANIZATION NAME(S) AND ADDRESS(ES) Washington University Research Office, Campus Box 1054 One Brookings Drive St. Louis MO 63130		10. SPONSORING / MONITORING AGENCY REPORT NUMBER  RL-TR-96-64		
9. SPONSORING / MONITORING AGENCY NAME(S) AND ADDRESS(ES) Rome Laboratory (OCPA) 26 Electronic Pky Rome NY 13441-4515				
11. SUPPLEMENTARY NOTES  Rome Laboratory Project Engineer: Raymond Boncek/OCPA/(315)330-2937				
12a. DISTRIBUTION / AVAILABILITY STATEMENT  Approved for public release; distribution unlimited.		12b. DISTRIBUTION CODE		
13. ABSTRACT (Maximum 200 words)  This report examines the design and fabrication of poled films of electro-optic materials utilizing photopolymerizable organic polymers. Background information on the theory of electro-optic activity and the salient design parameters necessary for deciding whether the material is a good candidate for a planar electro-optic modulator is presented. The details of the material processing, material characterization and fiber coupling are described including the preparation of guest-host mixtures that result in single-mode polymer waveguides (2=1300 nm) with core dimensions approximately equal to those of single-mode fiber. Experimental results of $r_{33}$ measurements are presented for DRI and DRI3 materials and several possible sources of electro-optic activity improvements are discussed.				
14. SUBJECT TERMS Electro-optic effect, Non-linear optic, Electro-optic modulators, DRI, DRI3, Optical Waveguides, Polymers, Fiber-to-waveguide couple, D-fiber		15. NUMBER OF PAGES 28		16. PRICE CODE
17. SECURITY CLASSIFICATION OF REPORT UNCLASSIFIED	18. SECURITY CLASSIFICATION OF THIS PAGE UNCLASSIFIED	19. SECURITY CLASSIFICATION OF ABSTRACT UNCLASSIFIED	20. LIMITATION OF ABSTRACT UL	

## TABLE OF CONTENTS

SECTION	PAGE
1 Introduction	1
2 Coupling Single-Mode Optical Subsystems Efficiently	1
3 Calculating $r_{13}$ , $r_{23}$ and $r_{33}$ from Intensity vs. Voltage Curves	3
4 Measurement of $r_{33}$	8
5 Uncertainties in $r_{33}$ Measurements	9
6 Discussion	10
7 Back Projection Technique	12
8 Summary	16
List of References	17

## LIST OF FIGURES

FIGURE	PAGE
1      Schematic of D-fiber, transcision, and alignment ways used for coupling singlemode optical fiber to polymer waveguides	3
2      Set-up to measure transmission of optical power as a function of modulation voltage	4
3      Modulator sample and coordinate axes	4
4      Picture on left shows physical model of sample, schematic on right show equivalent circuit model	11
5      Back projection process diagram	13
6      Acrylic core layer of “y”-branch showing definition of side-walls when layer has been exposed in N <sub>2</sub> ambient by Oriel UV lamp	14
7      SEM of the “Y” branch of the trench for an optical waveguide	14
8      SEM of PMMA waveguide cross-section using blade technique to fill the trench with the core NLO material (1500-46)	16

## LIST OF TABLES

TABLE		PAGE
1	Refractive index of poled DR1 in PMMA	8
2	Uncertainties in device parameters and effect on $r_{33}$	9
3	NLO chromophores	12
4	Back projection process steps	15

# **A Study of Poled Films of Advanced Electrooptic Polymers**

## **Final Progress Report**

---

Submitted by:

*Robert R. Krchnavek & Daniel L. Rode*  
Optoelectronics Research Laboratory  
Department of Electrical Engineering  
Washington University  
St. Louis, Missouri 63130-4899

Rome Laboratory Program Manager:

*Dr. Raymond K. Boncek*  
Rome Laboratory  
Rome, New York 13441-4515

---

Robert R. Krchnavek

Campus Box 1127  
telephone: 314-935-4896  
E-mail: *rrk@ee.wustl.edu*

Daniel L. Rode

Campus Box 1127  
telephone: 314-935-5575  
E-mail: *dlr@ee.wustl.edu*

Raymond K. Boncek

Rome Laboratory  
telephone: 315-330-2937  
E-mail: *boncek@rl.af.mil*

**Expert Science & Engineering Program**  
**Rome Laboratory BAA 93-07-PKRZ**  
**Major Areas (1), (3) and (4)**  
**Duration: 12 months**

## 1. Introduction

Efficient coupling to polymer waveguides is important to properly test the optical systems and subsystems for integrity and electrooptic effects. Toward this end, high coupling techniques have been developed by incorporating single-mode optical fibers and single-mode acrylic waveguides. This technique will be reviewed briefly. Using an optical set-up to measure the optical intensity that exits polymer waveguides,  $r_{ij}$  electrooptic coefficients can be calculated. The calculations necessary are described in detail. For modulation, it is necessary to apply the correct bias voltage to the NonLinear Organic (NLO) materials.  $V_{\pi}$  is measured so that a system can be designed and tested. Also, uncertainties in the  $r_{33}$  calculation are reviewed in order to note the effects that may degrade or improve the electrooptic effect of the NLO material. The final section presents the experimental work carried out to study the nonlinear optical polymers including valuable insights to processing and handling of these materials.

## 2. Coupling Single-Mode Optical Subsystems Efficiently

Optical sub-systems incorporating single-mode optical waveguides have several valuable features. Connections from single-mode fibers to single-mode waveguides can be made efficiently because of the NA matching. Some optical components require single-mode operation. Examples include electrooptic modulators and wavelength division demultiplexers. Because such components are expected to play a vital role in future electronic systems, high efficiency coupling is essential.

When launching light into a single-mode waveguide, care must be taken to match the NA of the source with that of the waveguide and to match the physical geometries. With a larger mismatch in NA between optical components, the coupling efficiency decreases. An approximate efficiency of coupling optical energy between two confined beams can be determined by knowing the mode field diameter. As the NA of the source and the NA of the waveguide are matched and the physical apertures are matched, optical power will be transferred to the optical waveguide with high efficiency.

Single-mode optical fiber is used to launch and receive optical power from single-mode optical waveguides. The fiber has an 8  $\mu\text{m}$  core with a 125  $\mu\text{m}$  outer diameter. The coupling technique relies on the combination of three factors: a modified single-mode fiber that is lapped to the core; photodefined alignment ways to guide the modified fiber; and a transcision at the waveguide face to expose the waveguide to the modified fiber. Refer to Fig. 1 for a schematic representation of the coupling technique noting the three related factors. As noted in Fig. 1, the buried acrylic waveguide does not extend to the substrate edge as it would in a typical butt-coupling scheme. Instead, the lower cladding extends beyond the input of the buried acrylic waveguide. If the fiber is lapped to the core from one direction and then cleaved and polished, the lapped region can be laid on the lower cladding layer between the alignment ways so the core of the fiber will be at the same height as the waveguide. After cleaving the lapped single-mode fiber and polishing the end face, the cross section resembles a "D" in shape.



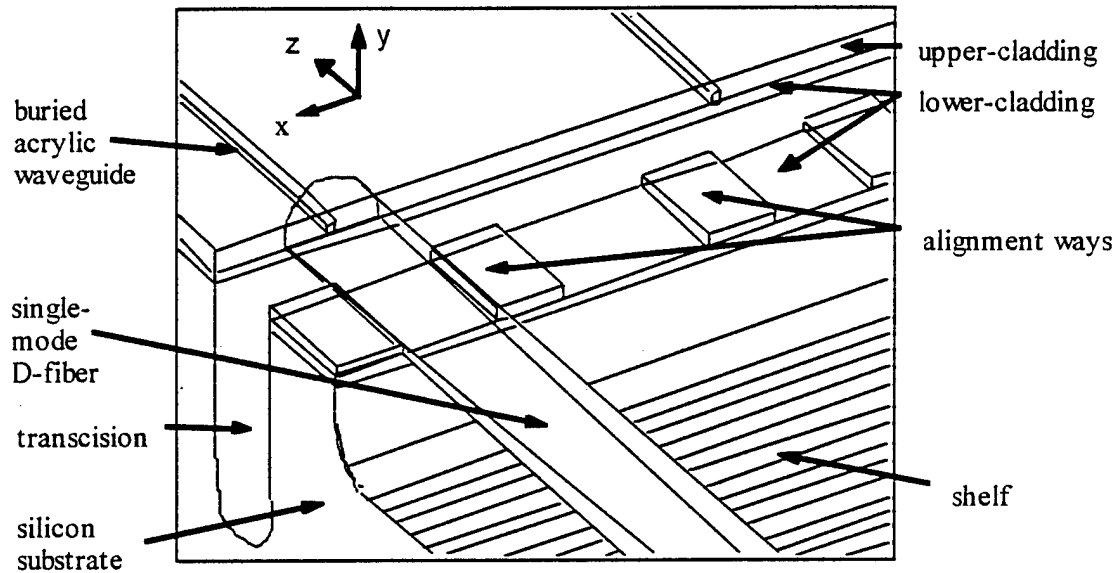


Fig. 1. Schematic of D-fiber, transcision, and alignment ways used for coupling single-mode optical fiber to polymer waveguides.

The combination of a precisely lapped D-fiber and a lower cladding layer results in controlling the  $y$ -variable in the coupling scheme. The  $x$ -variable is controlled by the precise positioning of the alignment ways which are photo-processed with the same mask used to photo-process the optical waveguides. By carefully placing a transcision between the alignment ways and the buried acrylic waveguides perpendicular to the optical axis, the D-fiber can be slid on the lower cladding between the alignment ways directly to the near vertical ( $\sim 0.75^\circ$  tilt) end face of the acrylic waveguide. All these position-controlling features help to place the single-mode D-fiber in the appropriate location for optimal coupling. Using the cut-back technique, an average excess coupling loss of 0.25 dB between single-mode D-fiber and single-mode acrylic waveguide was measured.<sup>1</sup> Next, we consider the electrooptic qualities of the single-mode acrylic waveguides.

### 3. Calculating $r_{13}$ , $r_{23}$ and $r_{33}$ from Intensity vs. Voltage Curves

Previously we presented<sup>2</sup> data for the intensity of light transmitted through the transverse modulator versus applied modulation voltage. This section shows how to convert these voltage curves into measurements of the material  $r_{13}$ ,  $r_{23}$  and  $r_{33}$  values. The measurements were made using the following optical set-up as shown in Fig. 2. The transverse modulator measures the phase shifts of the vertically polarized light ( $E$ -vector perpendicular to slab waveguide) relative to the horizontally polarized light ( $E$ -vector parallel to the slab).

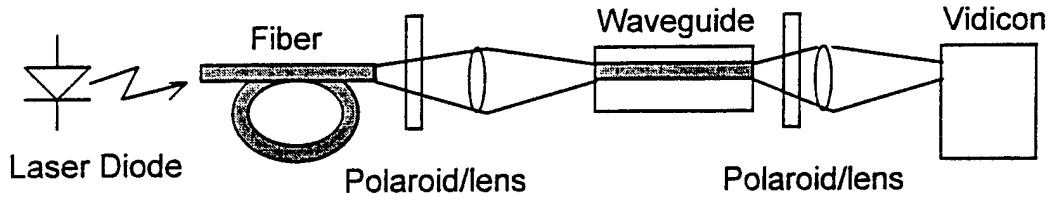


Fig. 2. Set-up to measure transmission of optical power as a function of modulation voltage.

The coordinate axes used in this derivation are shown in Fig. 3.

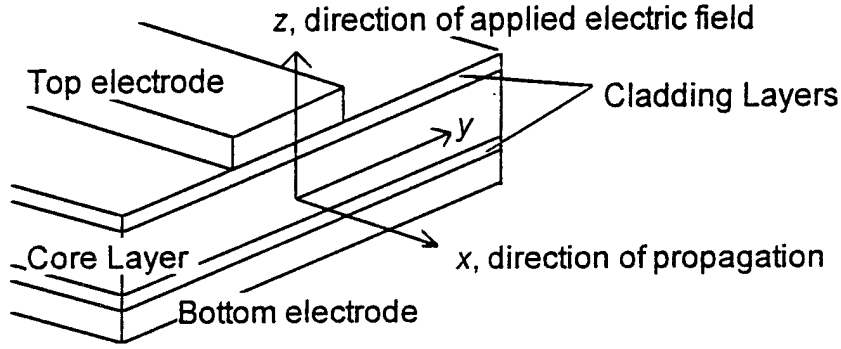


Fig. 3. Modulator sample and coordinate axes.

The resulting intensity observed beyond the second polarizer is:

$$I = \frac{I_{max}}{2} (1 + \cos(\phi_y - \phi_z)) \quad (1)$$

where  $\phi_y$  and  $\phi_z$  are the phase shifts of the horizontal and vertically polarized light respectively, and  $I_{max}$  is the maximum intensity. The problem is to relate  $\phi_y$  and  $\phi_z$  to the material properties  $r_{13}$ ,  $r_{23}$ ,  $r_{33}$  and the applied electric field  $E_z$ .

The index of refraction ellipsoid can be described for the completely general case as:<sup>3</sup>

$$a_{11}n_x^2 + a_{22}n_y^2 + a_{33}n_z^2 + 2a_{23}n_y n_z + 2a_{13}n_x n_z + 2a_{12}n_x n_y = 1 \quad (2)$$

where the  $a$ -coefficients are given by equation (3).

$$\begin{bmatrix} a_{11} \\ a_{22} \\ a_{33} \\ a_{23} \\ a_{13} \\ a_{12} \end{bmatrix} = \begin{bmatrix} \frac{1}{n_{x0}^2} \\ \frac{1}{n_{y0}^2} \\ \frac{1}{n_{z0}^2} \\ 0 \\ 0 \\ 0 \end{bmatrix} + \begin{bmatrix} r_{11} & r_{12} & r_{13} \\ r_{21} & r_{22} & r_{23} \\ r_{31} & r_{32} & r_{33} \\ r_{41} & r_{42} & r_{43} \\ r_{51} & r_{52} & r_{53} \\ r_{61} & r_{62} & r_{63} \end{bmatrix} \cdot \begin{bmatrix} E_x \\ E_y \\ E_z \end{bmatrix} \quad (3)$$

The indices of refraction for light polarized along their respective axis with no external electric field applied are  $n_{x0}$ ,  $n_{y0}$  and  $n_{z0}$ . The modulating electric fields are  $E_x$ ,  $E_y$ , and  $E_z$ , and the  $r_{ij}$  elements of matrix are the electrooptic coefficients (this formulation assumes that the  $x$ ,  $y$  and  $z$  axes have been aligned with the principal axes).

These expressions are general, but for our measurement situation and material, they can be simplified. First, as the material will be poled with an electric field applied through the sample (in the  $z$ -direction), and the material is isotropic except for this poling, the principle  $z$ -axis will be perpendicular to the slab, and the  $x$ - and  $y$ -axes will be equivalent. Therefore  $r_{1x}$  and  $r_{2x}$  coefficients will be equal to each other. Also,  $E_x$  and  $E_y$  are zero, because we do not apply any electric field in the plane of the modulator. Finally, because the two polarizations of light of interest are perpendicular and parallel to the slab, and as these are each principal axes of the material, we do not need to worry about the cross terms ( $a_{23}$ ,  $a_{13}$ ,  $a_{12}$ ).

The general equations then reduce to:

$$\begin{aligned} a_{22}n_y^2 &= 1 \quad \text{for horizontal polarization} \\ a_{33}n_z^2 &= 1 \quad \text{for vertical polarization} \end{aligned} \quad (4)$$

and

$$\begin{bmatrix} a_{11} \\ a_{22} \\ a_{33} \end{bmatrix} = \begin{bmatrix} \frac{1}{n_{x0}^2} \\ \frac{1}{n_{y0}^2} \\ \frac{1}{n_{z0}^2} \end{bmatrix} + \begin{bmatrix} r_{23} \\ r_{23} \\ r_{33} \end{bmatrix} E_z \quad (5)$$

Solving these equations for  $n_y$  and  $n_z$  gives:

$$\begin{aligned} n_y &= \frac{1}{\sqrt{\frac{1}{n_{y0}^2} + r_{23}E_z}} \\ n_z &= \frac{1}{\sqrt{\frac{1}{n_{z0}^2} + r_{33}E_z}} \end{aligned} \quad (6)$$

The phase shift for each polarization is then

$$\begin{aligned} \phi_y &= 2\pi \frac{n_y l}{\lambda} = 2\pi \frac{l}{\lambda \sqrt{\frac{1}{n_{y0}^2} + r_{23}E_z}} \quad \text{for the horizontal polarization} \\ \phi_z &= 2\pi \frac{n_z l}{\lambda} = 2\pi \frac{l}{\lambda \sqrt{\frac{1}{n_{z0}^2} + r_{33}E_z}} \quad \text{for the vertical polarization} \end{aligned} \quad (7)$$

where  $l$  is the length of the transverse modulator and  $\lambda$  is the wavelength of light in the material. The difference in phase shift between the two polarizations is therefore

$$\phi_y - \phi_z = 2\pi \frac{l}{\lambda} \left( \frac{1}{\sqrt{\frac{1}{n_{y0}^2} + r_{23}E_z}} - \frac{1}{\sqrt{\frac{1}{n_{z0}^2} + r_{33}E_z}} \right) \quad (8)$$

When there is no applied modulation voltage ( $E_z$  is zero) the initial phase difference is

$$\Delta\phi_0 = 2\pi \frac{l}{\lambda} (n_{y0} - n_{z0}) \quad (9)$$

When a voltage is applied that causes a phase shift of  $\pi$  radians from this value, the phase difference is

$$\Delta\phi_{\pi} = 2\pi \frac{l}{\lambda} \left( \frac{1}{\sqrt{\frac{1}{n_{y0}^2} + r_{23} \frac{V_{\pi}}{h}}} - \frac{1}{\sqrt{\frac{1}{n_{z0}^2} + r_{33} \frac{V_{\pi}}{h}}} \right) = \Delta\phi_0 + \pi \quad (10)$$

where  $h$  is the thickness of the structure between the electrodes. Note that we assume the core and cladding layers have infinite resistance and the electric field is  $V_{\pi}/h$ . It is now advantageous to make the approximation that  $r_{23}$  and  $r_{33}$  are typically very small compared to  $n_{y0}$  and  $n_{z0}$ .<sup>2,5</sup> The square root can therefore be approximated by the first two terms of a Taylor series. The result is

$$2\pi \frac{l}{\lambda} (n_{y0} - n_{z0}) + \pi = 2\pi \frac{l}{\lambda} \left( n_{y0} - r_{23} n_{y0}^3 \frac{V_{\pi}}{h} - n_{z0} + r_{33} n_{z0}^3 \frac{V_{\pi}}{h} \right) \quad (11)$$

$$\text{or} \quad \pi = 2\pi \frac{l}{\lambda} (-r_{23} n_{y0}^3 + r_{33} n_{z0}^3) \frac{V_{\pi}}{h} \quad (12)$$

We now have four unknowns, the  $r_{ij}$  coefficients and the indices of refraction along the two axes. We have not measured  $n_{y0}$  or  $n_{z0}$  for these materials after poling. However, we can make reasonable estimates based on previous measurements and published information. Page<sup>4</sup> presents data showing that 5 to 10% of Disperse Red #1 (DR1) in Poly-Methyl MethAcrylate (PMMA) increases the index of refraction of the resin by +0.0218 before poling. What we require, however, is the indices after poling. We expect  $n_{z0}$  to increase and  $n_{y0}$  to decrease from the initial unpoled index. The magnitude of the change will depend on how efficiently the sample is poled. In the best case, where all the dye molecules are perfectly aligned along the  $z$ -axis, we would expect  $n_z$  to increase by three times the change caused by the unpoled dye. If  $n_{z1}$  is the index of the resin itself (without dye) and  $n_{z2}$  is the index of the unpoled resin with dye, then  $n_{z3}$  is the perfectly poled  $z$ -axis refractive index.

$$\begin{aligned} n_{z3} &= n_{z1} + 3(n_{z2} - n_{z1}) \\ n_{y3} &= n_{y1} = n_{z1} \end{aligned} \quad (13)$$

However, published results suggest that at best only a small fraction of the molecules are reoriented during poling.<sup>5</sup> Several reports<sup>6,7</sup> have derived a three to one ratio for  $r_{33}/r_{23}$ , based on the physics of the poling process. What is seldom mentioned when referring to this 3:1 ratio is that it only holds for weak poling. Measured data in the literature shows ratios from 2:1 to 4:1.<sup>8</sup> We can reasonably assume about a 3:1 ratio for our experiment, and for the relative changes in  $n_z$  and  $n_y$  during poling.

Teng<sup>5</sup> did an experiment with P2ANS attached to MMA in which they measured  $n_y$  and  $n_z$  as a function of applied field during poling. Although this is not the same system as ours, their results suggest that the refractive index changes during poling are small compared to the change in index due to the dye being added to the resin. Comparing their results to ours, we can estimate how much  $n_y$  and  $n_z$  will change after poling. Based on these arguments, our best estimate of  $n_{y0}$  and  $n_{z0}$  are shown in Table 1.

Index	Resin	Dye	Poling	Total
$n_{y0}$	= 1.494 +	0.0218 -	0.0058 =	1.51
$n_{z0}$	= 1.494 +	0.0218 +	0.0131 =	1.5289

Table 1. Refractive index of poled DR1 in PMMA

Likewise, we assume the usual 3:1 ratio of  $r_{33}/r_{23}$ , that is,

$$r_{23} = \frac{r_{33}}{3} \quad (14)$$

Plugging these into equation (12) gives,

$$|r_{33}| = \frac{\lambda h}{2IV_\pi \left( n_{z0}^3 - \frac{n_{y0}^3}{3} \right)} = \frac{\lambda h}{4.82IV_\pi} \quad (15)$$

This is the equation used to calculate the  $r_{33}$  results presented below.

#### 4. Measurement of $r_{33}$

From the formula for intensity versus phase shifts shown in (1) and the relationship between the phase shift for polarization and electric field as derived in (7), we expect the intensity to vary sinusoidally with modulation voltage:

$$I = \frac{I_{max}}{2} (1 + \cos(2\pi \frac{V}{V_\pi} + \phi_0)) \quad (16)$$

The data we obtained represented a portion of this curve. To calculate  $r_{33}$  we need a measure of optical power, applied voltage and polarization angle. Using this data, a least squares fit with the parameters  $I_{max}$ ,  $V_\pi$  and  $\phi_0$  can be made. The resulting  $V_\pi$  can then be inserted into (15) to give  $|r_{33}|$ . Combining the measurements made on samples as reported previously<sup>9</sup> and the preceding equations, we can calculate the electrooptic coefficient  $|r_{33}|$  when using the following chromophores in the guest-host system.

$$\text{DR1: } |r_{33}| = 0.445 * 10^{-12} \text{ m/V}$$

$$\text{DR13: } |r_{33}| = 0.561 * 10^{-12} \text{ m/V}$$

### 5. Uncertainties in $r_{33}$ Measurements

There are six values that go into this  $r_{33}$  calculation: the sample thickness  $h$ , the wavelength  $\lambda$ , interaction length  $l$ ,  $V_\pi$  and the indices of refraction  $n_{y0}$  and  $n_{z0}$ . We can analyze for the effect of each of these separately and then RSS (Root Sum of the Squares) these effects together to give a maximum uncertainty.

As an example of this analysis for the uncertainty in thickness,

$$|r_{33}| = \frac{\lambda h}{2 \left( n_{z0}^3 - \frac{n_{y0}^3}{3} \right) l V_\pi}, \text{ so} \quad (17)$$

$$\delta|r_{33}| = \left| \left( \frac{\partial}{\partial h} r_{33} \right) \delta h \right| = \left| \frac{\lambda}{2 \left( n_{z0}^3 - \frac{n_{y0}^3}{3} \right) l V_\pi} \delta h \right| \quad (18)$$

For these samples, we estimate the uncertainty in our thickness measurement as being about  $0.5 \mu\text{m}$  for the DR1 sample. Therefore the uncertainty in  $r_{33}$  due to uncertainty in our thickness measurement is  $8.89 * 10^{-15}$  for the DR1 sample. Using a similar analysis for the other variables results in the values shown in Table 2.

Variable	DR1		DR13	
	Uncertainty	$\delta r_{33} $	Uncertainty	$\delta r_{33} $
$h$	$\pm 0.5 \mu\text{m}$	$8.89 * 10^{-15}$	$\pm 1.0 \mu\text{m}$	$2.34 * 10^{-14}$
$\lambda$	$\pm 0.001 \mu\text{m}$	$3.37 * 10^{-16}$	$\pm 0.001 \mu\text{m}$	$4.27 * 10^{-16}$
$l$	$\pm 0.5 \text{ mm}$	$5.29 * 10^{-15}$	$\pm 0.5 \text{ mm}$	$1.04 * 10^{-14}$
$V_\pi$	$\pm 34 \text{ V}$	$2.07 * 10^{-14}$	$\pm 25 \text{ V}$	$1.62 * 10^{-14}$
$n_{y0}$	$\pm 0.013$	$5.44 * 10^{-15}$	$\pm 0.013$	$6.87 * 10^{-15}$
$n_{z0}$	$\pm 0.013$	$1.67 * 10^{-14}$	$\pm 0.013$	$2.11 * 10^{-14}$

Table 2. Uncertainties in device parameters and effect on  $r_{33}$

The value for  $r_{33}$  with the calculated uncertainty (RSS of the uncertainties) for each chromophore is then:

$$|r_{33}(\text{DR1})| = (0.445 \pm 0.029) * 10^{-12} \text{ m/V}$$

$$|r_{33}(\text{DR13})| = (0.561 \pm 0.038) * 10^{-12} \text{ m/V}$$

## 6. Discussion

Through July, our experimental work was concentrated on improving the  $r_{33}$  results with DR1 and DR13. Unfortunately the above results are the best we could get. There are several possible explanations:

- Low dye concentration
- Poor poling efficiency
- Conductivity differences between the core and cladding layers
- Fast relaxation of the order induced during poling<sup>10</sup>
- UV degradation
- Dye resin interaction (including dye-photo initiator interaction)

Attempts to increase the concentration of DR13 in the acrylic resulted in films that did not transmit light. Viewing the samples by eye, the higher concentration films looked dull indicating a rough surface. It appears that with a concentration above 5%, the DR13 and acrylic phase segregate producing higher scattering and loss.

We made several attempts to improve the poling process. We tried poling for a longer time with a slower temperature ramp and at a higher temperatures. These produced no significant improvement.

In one significant experiment we applied heat and electric field to the sample as we passed light through it. At 125°C and 300 volts (about 10 volts/ $\mu\text{m}$  field strength) we observed significant absorption of the vertically polarized light, but not the horizontal. When allowed to cool, the vertical transmission returned. This result suggests that whatever poling action was taking place in the sample when hot was not stable at room temperature.

Another interesting result on this sample was the time behavior of the transmission. If the sample is at room temperature with no voltage, a baseline transmission of light was observed. When a voltage was applied, the transmission quickly increased and then faded away again with about a one minute time constant.

This result suggested to us that a difference in conductivity between the core and cladding could be causing the ineffective poling. The problem is illustrated in Fig. 4.

The conductivity of the core and cladding will tend to discharge the effective capacitance of each layer. If all the resistances are proportional to the thickness of the layer, the voltages will still be divided as we expect. If the core has a higher conductivity than the cladding, it will discharge, leaving most of the voltage across the cladding. The result is that the core has less electric field than expected which results in a significantly reduced electrooptic effect for the applied voltage.

To directly test the conductivity theory, we made a new sample with just the core material on un-oxidized silicon. After sputtering a gold electrode onto the top surface, the



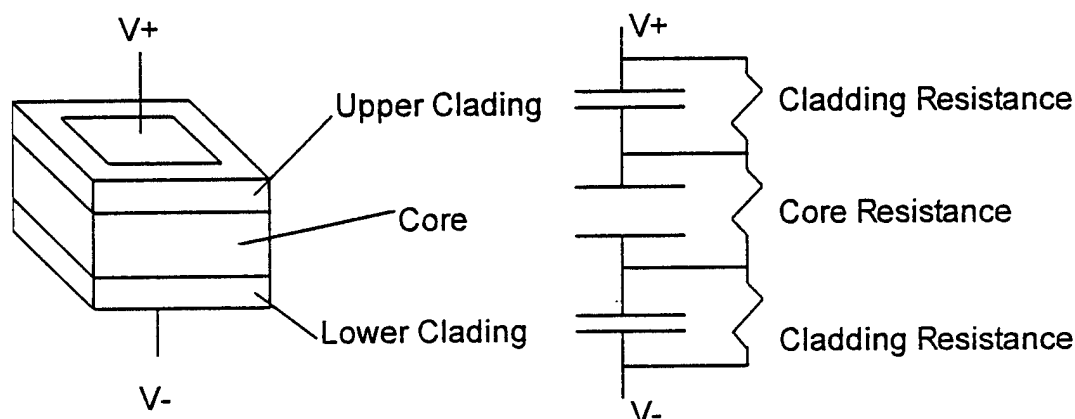


Fig. 4. Picture on left shows physical model of sample, schematic on right shows equivalent circuit model.

resistance of the film was measured at 100 volts. The result was a current of  $0.5 \mu\text{A}$  for a film area of  $1.96 \times 10^{-3} \text{ m}^2$  and thickness  $10 \mu\text{m}$ . If the cured resin has a dielectric constant of 2.5, the RC time constant for the core film would be about 1 second. Given that conductivity of these films may be highly process dependent, this agrees with the observed one minute time constant. As all previous measurements were made essentially DC, this conductivity could well be an explanation for some of our  $r_{33}$  discrepancy.

Core conductivity will have an adverse effect during poling also. Poling is inherently a DC field process. If the core conducts and the cladding does not, then the core will not see a large poling field and little reorientation will take place. We know from experience that the undoped cladding layers we have used so far have high resistance. The samples remain charged for several minutes after removing them from the corona poling field. If the core is conducting, then there is little doubt that most of this field is across the cladding layers instead of the core.

These results all suggest that this particular guest-host system is too unstable to be used in real devices. For a practical device we need a material that is stable at room temperature and at the moderately high temperatures common inside electronic units. Many results have suggested that covalently bound chromophore-resin systems show much better stability at room temperature than guest-host systems. At elevated temperatures the important parameter is the glass transition temperature,  $T_g$ . Therefore, we resumed a study started earlier in the year to find the most promising covalently bound chromophore-resin systems reported. Some of the most promising systems are shown in Table 3.

None of these materials are photodefinable. There is growing opinion that effective NLO chromophores will all be too sensitive for photo-definition with Ultra-Violet (UV) light. For HCC-1232, no devices are reported to have been made, only a thin film

Material	$n$	Reported $r_{33}$	Measurement	Reference
HCC-1232 $T_g = 135^\circ\text{C}$	1.63 @ 1.34 $\mu\text{m}$	38 pm/V @ 1.34 $\mu\text{m}$	thin-film ellipsometry	Haas <sup>11</sup>
PUR-DR19 polyurethane	1.753 @ 633 nm 1.692 @ 800 nm	12 pm/V @ 1.06 $\mu\text{m}$	Mach-Zehnder modulator	Wang <sup>12</sup>
1500-46 $T_g = 203^\circ\text{C}$	1.745 @ 589 nm 1.61 @ 1.3 $\mu\text{m}$	8.5 pm/V @ 1.3 $\mu\text{m}$	Mach-Zehnder modulator	Stenger-Smith <sup>13</sup>

Table 3. NLO chromophores

measurement. One has to wonder whether this material has a low enough loss to make a practical device. The DR19-PolyUREthane material, on the other hand, has been made into a device. Furthermore, the synthesis steps for this material have been published,<sup>14</sup> allowing us to make it ourselves if needed. The 1500-46 material has a high  $T_g$  as compared to our acrylics (which start to decompose at  $185^\circ\text{C}$ ), however, sub- $T_g$  poling has been demonstrated. Another plus for this material is that it has been made into a modulator at 633 nm.<sup>15</sup>

Our main conclusion from this study is that the ideal NLO material has not been published yet. The key problem in this field is to discover an NLO material that has high  $r_{33}$ , moderate  $T_g$ , good stability below  $T_g$ , and low optical absorption.

## 7. Back Projection Technique

Based on the results presented above, we decided to develop a process for conveniently using a nonphotodefinable material in a practical device. The China Lake and USC groups that made modulators with their materials used a reactive ion etch process. They formed the base cladding layer and then a continuous core layer. Then, they etched away the unwanted core and surrounded it with upper- and side-cladding. The addition of a photodefinable procedure would increase flexibility in device fabrication.

We wanted to try a photodefinable process to form a trench that could be flooded with the core material. By appropriately controlling viscosity and the method of application, it should be possible to substantially fill the trench without getting too thick of a layer above the trench. The processing can be divided into two steps: trench formation and trench filling. We began with trench formation.

Because our acrylic resins are sticky until cured, we could not use contact printing. We have used proximity printing in the past with mixed results. It is a difficult process due to the requirement to get the mask very close to the resin surface, and due to variations in the thickness of the resin film, particularly the edge bead.

We chose to try a back projection technique instead. This technique uses a substrate transparent to UV light. Aluminum is deposited on one side and then etched into the

desired pattern of waveguides using standard photolithographic processes. Then a lower cladding layer is spun on and cured with a UV lamp from above the surface. This cures a full area layer 1 to 10  $\mu\text{m}$  thick. Next, the middle cladding layer is spun on. This time it is cured from below by passing the light through the aluminum layer, which acts as a mask one film thickness from the resin layer. After the device is formed, the aluminum traces can be used as electrodes for any active devices. This technique has the advantage of being a self-aligning process since the electrodes provide a mask to form the waveguides according to their design as shown in Fig. 5.

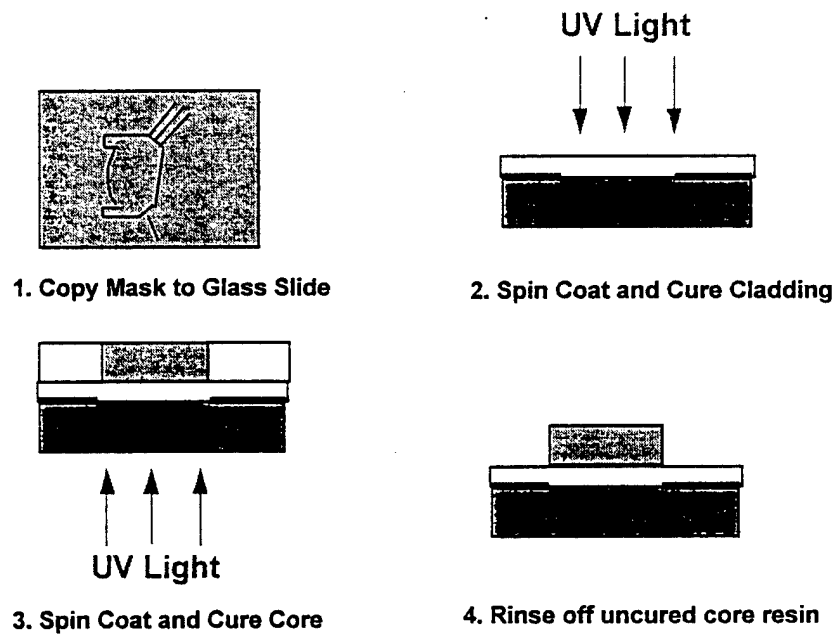


Fig. 5. Back projection process diagram.

Our first attempts with a Xenon arc lamp were unsatisfactory. We could not get the walls of the trenches to cure without the bottom of the trench partially curing also. The result was what looked like stringers or ribs across the trench which can be seen in Fig. 6. This problem was much worse for the narrow trenches than for the larger structures.

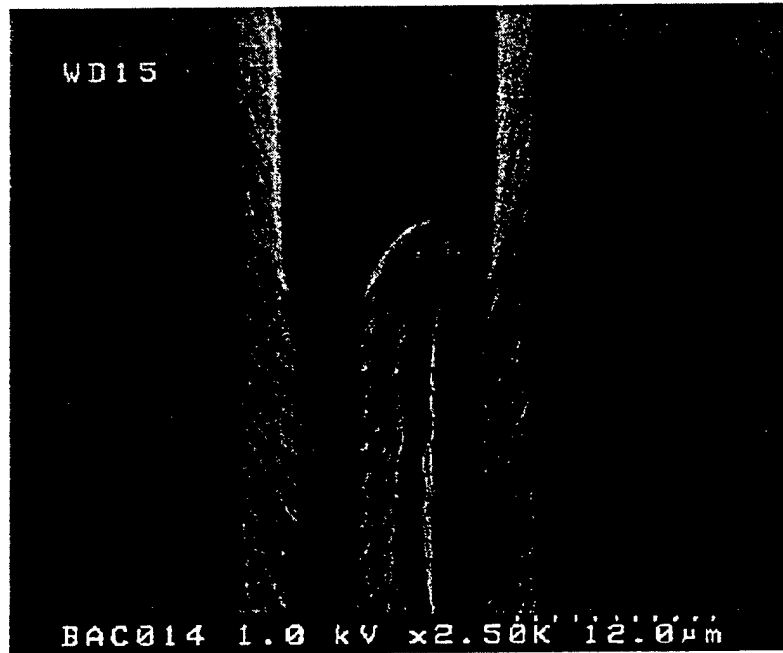
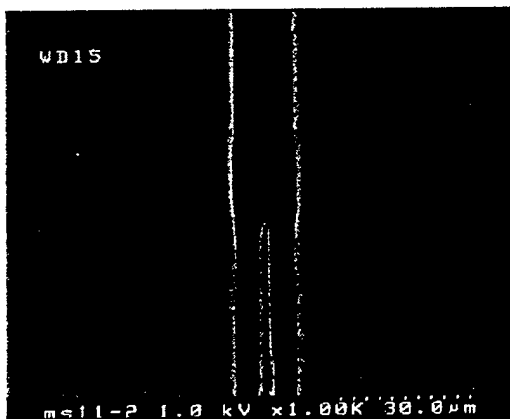
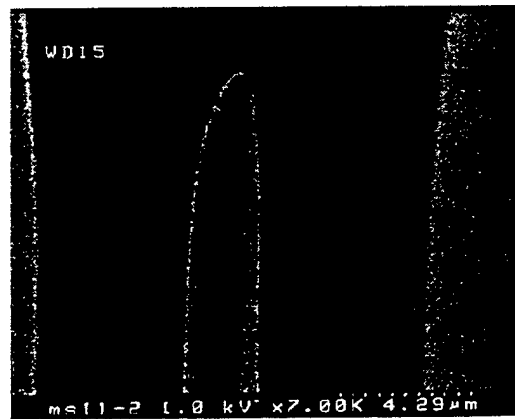


Fig. 6. Acrylic core layer of "Y"-branch showing definition of side-walls when layer has been exposed in  $N_2$  ambient by Oriel UV lamp. Back projection technique is used for this sample.

We next tried an Argon-ion laser ( $\lambda=350$  nm). This showed the same problem, but not as severe, until we tried a diffuser or mode-scrambler in the beam. A piece of adhesive tape was placed in the beam about 1 cm from the sample being exposed. A sample made this way is shown in Fig. 7. Note the smooth walls and excellent definition.



(a)



(b)

Fig. 7. SEM of the "Y" branch of the trench for an optical waveguide. (a) Improved quality of processing resolution due to Argon-ion exposure in air. (b) The enlargement of the central area of the branch in (a) showing the smooth side walls.

While perfecting this process, we also did many experiments with different development techniques. We tried room temperature acetone with ultrasonic agitation, warm (35°C) acetone with and without ultrasonic agitation, and spraying the acetone onto the sample with a squeeze bottle in the direction of the wave guides. The last technique ended up working adequately once the diffuser and proper exposure were discovered. The final back projection process is described in Table 4.

① Clean glass substrate
② Sputter Aluminum, about 0.1 $\mu\text{m}$ thickness
③ Define waveguides in Aluminum with standard, positive photo-resist processing
④ Etch Aluminum
⑤ Spin on lower-cladding, 4500 RPM, 90 seconds
⑥ Cure lower-cladding from above, 4 minutes of UV light at 45 mW/cm <sup>2</sup> in a N <sub>2</sub> ambient
⑦ Spin on middle-cladding, 3500 RPM, 90 seconds
⑧ Place sample on x-y stage, resin side down. Expose with Argon-ion laser, P=40mW, 7mm/sec scan speed, 400 $\mu\text{m}$ pitch, tape diffuser 1 cm from sample
⑨ Develop sample under an acetone stream

Table 4. Back projection process steps

While this process was being developed, we acquired<sup>16</sup> 500 mg of 1500-46 NLO polymer. This material has a molecular weight of 15 Kg/mole and a glass transition temperature of 203°C. Although the  $r_{33}$  of this material is not as high as some others reported, the high  $T_g$ , good  $r_{33}$  and the fact that it has been made into a modulator at 633 nm make this one of the leading materials presently available to us. It also is representative of the materials being investigated for NLO resins, and the handling and processing problems that will need to be solved.

To develop the process without spending all the NLO material, we started with 15,000 molecular weight PMMA dissolved in the solvents recommended by the manufacturing group (5% chlorobenzene in pyridine) for testing purposes. This proved difficult because of the low viscosity of the NLO material in the solvent system. At a spin speed high enough to get acceptable spreading, the film thickness was only a few microns thick. Even when mixed with less solvent, to produce a more viscous fluid, the films were very thin, with essentially the same thickness at the bottom of the trenches as on the surface. Even worse, the PMMA cracked during drying.

We next tried a blade technique. Instead of spinning the film to the required thickness, we used a glass slide to spread the fluid out and fill the trenches. The slide was then tilted on edge and lightly scraped across the substrate. The result was substantially more resin in the trenches which is shown in Fig. 8.

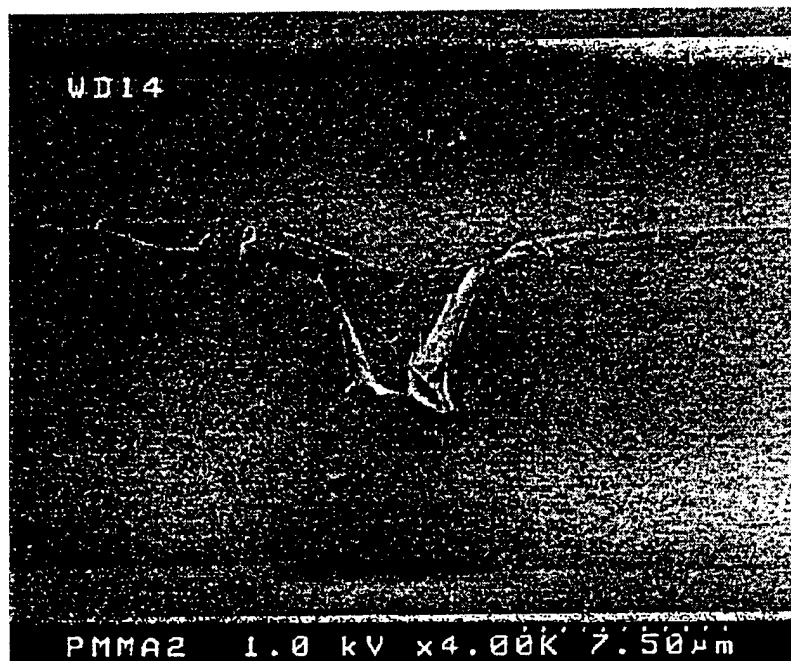


Fig. 8. SEM of PMMA waveguide cross-section using blade technique to fill the trench with the core NLO material (1500-46).

In discussions with the providers of the NLO material, they suggested that we would not have problems with cracking. The problems they had were in achieving a good film thickness and filling the trenches. Their modulator had waveguides with a cross section of about  $2\ \mu\text{m}$  square; ours are  $10\ \mu\text{m}$  square. The blade technique is giving us good results in this area.

## 8. Summary

We have demonstrated modulation using the DR-13 dye as a guest in our tri/di acrylate host. The result was somewhat disappointing in that the measured  $r_{33}$  values were lower than hoped for, and they faded within weeks at room temperature. Recent published results tend to confirm this for other guest-host systems as well; they have poor stability at room temperature.

Anticipating that the ideal NLO core material may not be photo-definable (because UV will damage the molecule), we developed a process for making and filling waveguide trenches with a nonphotodefinable resin. This new process has the advantages of being fast, giving good side wall smoothness, and automatic alignment of electrodes with the waveguides. This new process could have wide applicability to any NLO resin that can be put in solution. It also uses processes that are already widely used in the thick-film electronics industry.

- 
- <sup>1</sup> T. S. Barry, D. L. Rode, and R. R. Krchnavek, "Efficient Coupling Technique for Single-Mode Optical D-Fiber to Buried Polymer Acrylic Waveguide," *SPIE Photonic Device Engineering for Dual-Use Applications*, Orlando, FL, 17-18 April 1995, pp. 22-29.
- <sup>2</sup> R. R. Krchnavek and D. L. Rode, "Fundamental Characterization of Advanced Organic Polymers for Optical Waveguide Devices," Final Progress Report submitted to Rome Laboratory, 1994.
- <sup>3</sup> K. Lizuka, *Engineering Optics*, second edition, Springer-Verlag 1987.
- <sup>4</sup> R. H. Page, M. C. Jurich, B. Reck, A. Sen, R. J. Twieg, J. D. Swalen, G. C. Bjorklund, and C. G. Willson, "Electrochromic and optical waveguide studies of corona-poled electro-optic polymer films," in *J. Opt. Soc. Am., B*, vol. 7, No. 7, July 1990.
- <sup>5</sup> C. C. Teng, M. A. Mortazavi, and G. K. Boudoughian, "Origin of the poling-induced optical loss in a nonlinear optical polymeric waveguide," in *Appl. Phys. Lett.* 66 (6) February 1995.
- <sup>6</sup> M. G. Juzyk, K. D. Singer, H. E. Zahn, and L. A. King, "Second-order nonlinear-optical tensor properties of poled films under stress," in *J. Opt. Soc. Am. B*, vol. 6, no. 4, April 1989.
- <sup>7</sup> K. D. Singer, M. G. Kuzyk, and J. E. Sohn, "Second-order nonlinear-optical processes in orientationally ordered materials: relationship between molecular and macroscopic properties," in *J. Opt. Soc. Am. B*, vol. 4, No. 6, June 1987.
- <sup>8</sup> L. A. Hornak, "Polymers for Lightwave and Integrated Optics: Technology and Applications," Marcel Dekker, Inc. 1992, page 405.
- <sup>9</sup> See Ref. 2.
- <sup>10</sup> K. D. Singer, M. G. Kuzyk, W. R. Holland, J. E. Sohn, S. J. Lalama, R. B. Comizzoli, H. E. Katz, and M. L. Schilling, "Electro-optic phase modulation and optical second-harmonic generation in corona-poled polymer films," in *Appl. Phys. Lett.* 53 (19), 7 November 1988.
- <sup>11</sup> D. Haas, H. Yoon, H.-T. Man, G. Cross, S. Mann, N. Parsons, "Polymeric electro-optic waveguide modulator; materials and fabrication," SPIE vol. 1147, *Nonlinear Optical Properties of Organic Materials II*, pp. 222-232, 1990.
- <sup>12</sup> W. Wang, D. Chen, and H. R. Fetterman, "Traveling wave electro-optic phase modulator using cross-linked nonlinear optical polymer," *Appl. Phys. Lett.*, 65 (8), pp. 929-931, 22 August 1994.
- <sup>13</sup> Discussions with Geoffrey Lindsay and John D. Stenger-Smith (China Lake - Navy), Sample of high  $T_g$  Accordion NLO material (1500-46), September-December, 1995.
- <sup>14</sup> *ibid.*
- <sup>15</sup> *ibid.*
- <sup>16</sup> *ibid.*

***MISSION***  
***OF***  
***ROME LABORATORY***

**Mission.** The mission of Rome Laboratory is to advance the science and technologies of command, control, communications and intelligence and to transition them into systems to meet customer needs. To achieve this, Rome Lab:

- a. Conducts vigorous research, development and test programs in all applicable technologies;
- b. Transitions technology to current and future systems to improve operational capability, readiness, and supportability;
- c. Provides a full range of technical support to Air Force Materiel Command product centers and other Air Force organizations;
- d. Promotes transfer of technology to the private sector;
- e. Maintains leading edge technological expertise in the areas of surveillance, communications, command and control, intelligence, reliability science, electro-magnetic technology, photonics, signal processing, and computational science.

The thrust areas of technical competence include: Surveillance, Communications, Command and Control, Intelligence, Signal Processing, Computer Science and Technology, Electromagnetic Technology, Photonics and Reliability Sciences.